Supplementary Figures and Tables

"Testing the astronomical time scale for oceanic anoxic event 2, and its extension into Cenomanian Strata of the Western Interior Basin (USA)"

Chao Ma, Stephen R. Meyers, Brad B. Sageman, Brad S. Singer, Brian R. Jicha

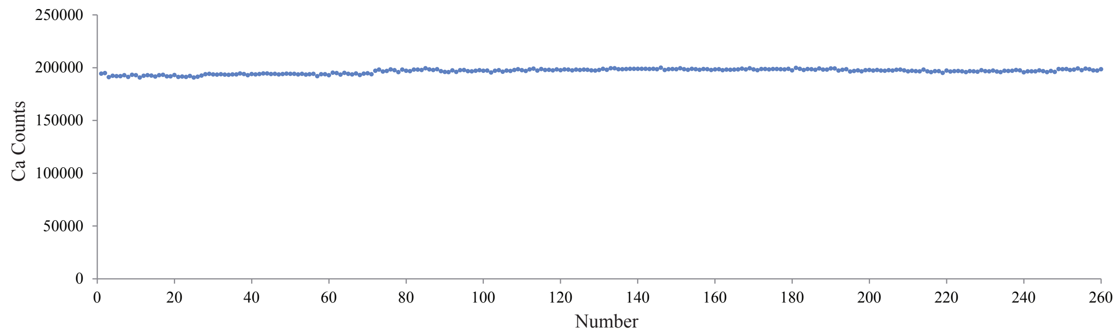

Fig. A.1. Stability of XRF scanner analyses during the period of the study. There are a total of 260 'monitor scans' of a laboratory standard ('SARM 4'; Potts et al., 1992), taken before and after each scanned core segment. This figure shows the Ca counts, which are very stable through time (the coefficient of variation is 0.01).

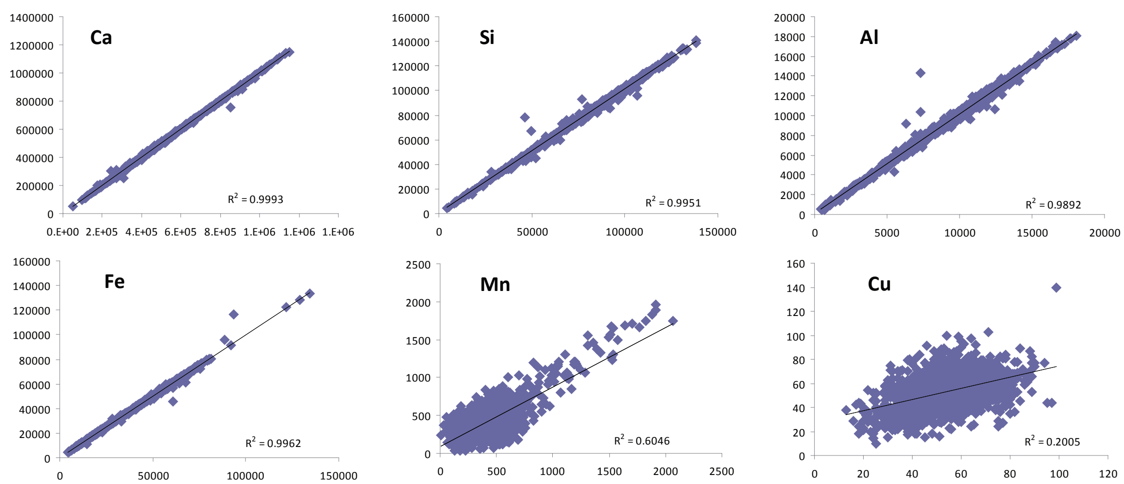

Fig. A.2. Cross plots of duplicate XRF analyses (counts vs. counts) of Angus core material analyzed in this study, for Ca, Si, Al, Fe, Mn and Cu.

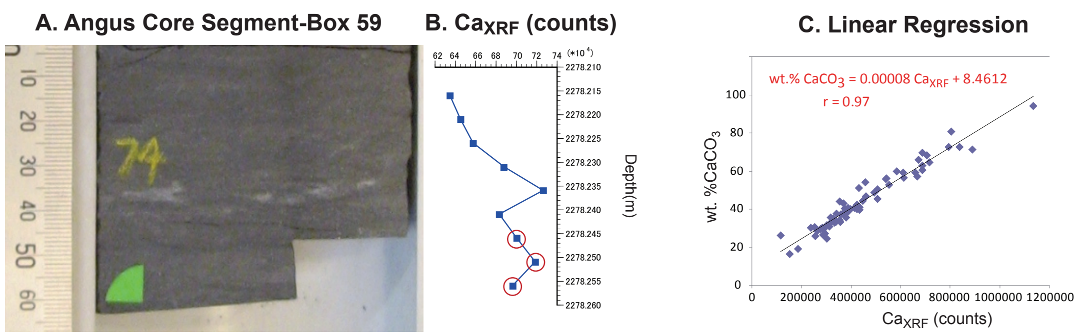

Fig. A.3. Calibration of calcium XRF scanning data to wt. % $CaCO_3$. (A) Image of a segment from box 59 of the Angus Core. The missing part in the lower right corner is the sample taken for measurement of wt. % $CaCO_3$ (68.34%) via CO_2 coulometry. The thickness of this segment is about 70 mm. (B) The XRF Ca counts for this interval of core (note that the units on the abscissa are 10^4 counts). The average value (705013.67 counts) of the three points (identified as red circles) is matched with the wt. % $CaCO_3$ (68.34%) determined from the sample via CO_2 coulometry. (C) The linear regression between the Ca counts and the wt. % $CaCO_3$ data yields y = 8E-05x + 8.4612, where y is wt. % $CaCO_3$ and x is Ca counts, r^2 = 0.94.

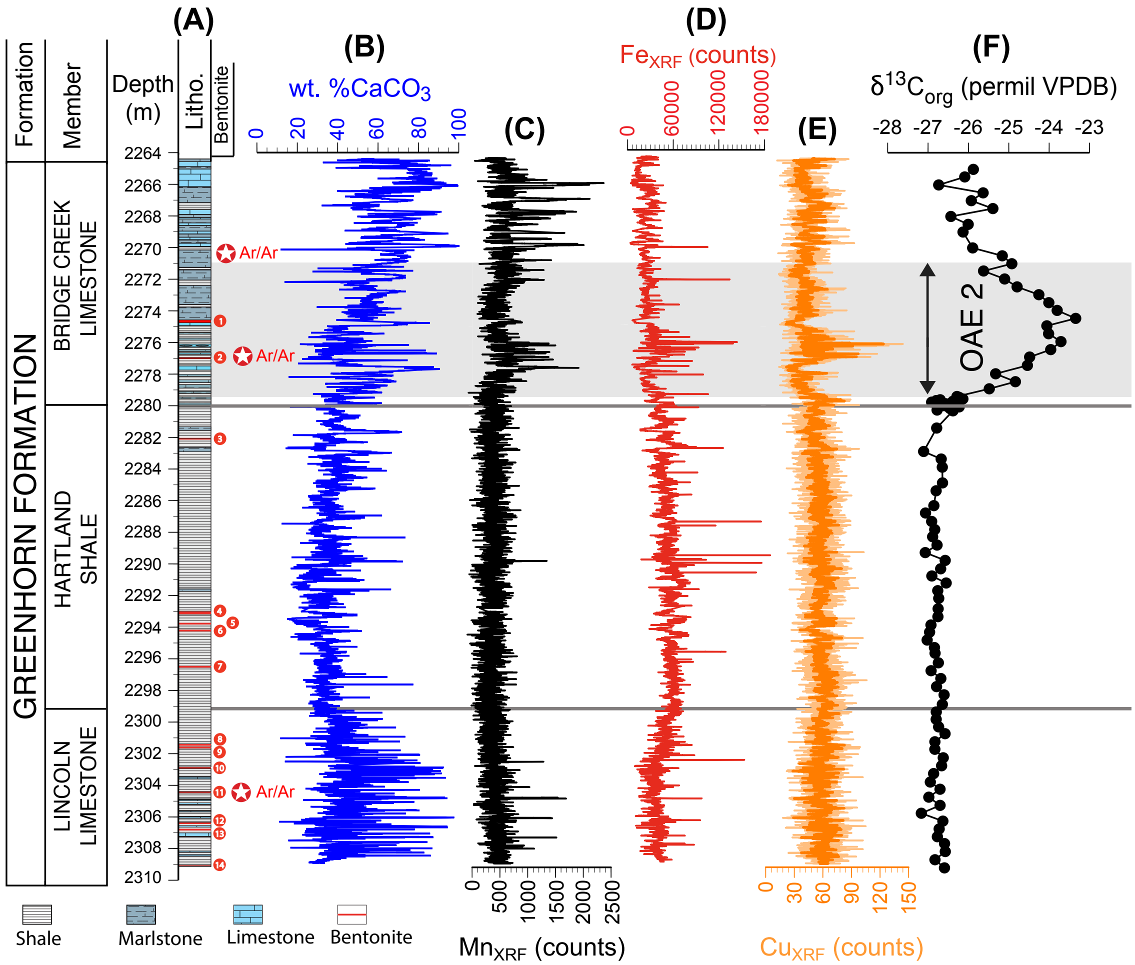

Fig. A.4. (A) Detailed stratigraphy for the Angus core. The numbered circles to the right of the stratigraphic column identify bentonite layers, and the three stars indicate the stratigraphic location of dated ash beds that have been correlated into the Angus core for geochronologic constraints. (B) Calibrated XRF wt.% $CaCO_3$ profile from this study, (C) XRF scanning results for Mn (counts). (D) XRF scanning results for Fe (counts). (E) XRF scanning results for Cu (counts) (the dark orange is smoothed with a Gaussian kernel). (F) Carbon isotope data from Joo et al. (2014). The shaded area indicates the interval of the OAE 2.

Table A.1. The mean coefficient of variation for duplicate measurements of core material from the Angus Core (Ca, Al, Si, Mn, Fe, Cu).

Element	Mean Coefficient of Variation	Standard Deviation of Coefficient of Variation	Number of duplicate measurements
Ca	0.005	0.009	1152
Al	0.019	0.026	1152
Si	0.014	0.016	1152
Mn	0.237	0.205	1148
Fe	0.008	0.012	1152
Cu	0.177	0.135	1152

Table A.2. Theoretical target periods used in the ASM analyses, based on the time domain astronomical model of Laskar et al. (2004, 2011). The uncertainty assessment is from Meyers et al. (2012b).

Term	Mean LA 04/LA 11 frequency (cycles/k.y.)	N^{δ}	Corresponding Laskar04/ Laskar11 period (k.y.)	2σ uncertainty (cycles/k.y.)	% Uncertainty in frequency
E1	2.466250×10^{-3}	4	405.47	5.737305×10^{-5}	2.3 %
E2	7.875000×10^{-3}	8	126.98	3.585686×10^{-4}	4.6 %
E3	1.031875×10^{-2}	8	96.91	4.307386×10^{-4}	4.2 %
O1	2.060000×10^{-2}	4	48.54	3.265986×10^{-4}	1.6 %
O2	2.655000×10^{-2}	4	37.66	2.000000×10^{-4}	0.8 %
P1	4.460000×10^{-2}	4	22.42	1.566312×10^{-3}	3.5 %
P2	5.455000×10^{-2}	4	18.33	2.000000×10^{-4}	0.4 %

δ = number of estimates used for determination of mean frequency and standard deviation.

Table A.3. Complete $^{40}Ar/^{39}Ar$ results relative to 28.201 Ma Fish Canyon sanidine

Sample: *D2315* J-value: 0.0153882 ± 0.04 (%1σ) D/amu: 1.0057 ± 0.04 (%1σ)

N	^{40}Ar (moles)	^{40}Ar (Volts)	± $1\sigma_{40}$ (Volts)	^{39}Ar (Volts)	± $1\sigma_{39}$ (Volts)	^{38}Ar (Volts)	± $1\sigma_{38}$ (Volts)	^{37}Ar (Volts)	± $1\sigma_{37}$ (Volts)	^{36}Ar (Volts)	± $1\sigma_{36}$ (Volts)	$\%^{40}Ar^*$	$^{40}Ar^*/^{39}Ar_K$	± 1σ	Age (Ma)	± 2σ (Ma)	K/Ca	Outliers
1	3.271E-15	0.554157	0.000645	0.146126	0.000236	0.001800	0.000058	0.001283	0.000069	0.000155	0.000006	91.76	3.479851	0.01336	95.49	± 0.71	49.0	< 95%*40Ar
2	7.067E-15	1.197404	0.000794	0.335728	0.000270	0.004059	0.000051	0.003658	0.000070	0.000107	0.000006	97.39	3.473587	0.00646	95.32	± 0.35	39.5	
3	5.283E-15	0.895107	0.000652	0.246838	0.000249	0.002949	0.000086	0.001952	0.000068	0.000130	0.000007	95.74	3.471893	0.00986	95.27	± 0.53	54.4	
4	3.747E-15	0.634885	0.000534	0.172570	0.000199	0.002106	0.000074	0.001637	0.000055	0.000097	0.000006	95.51	3.513736	0.01155	96.39	± 0.62	45.3	xenocryst
5	4.619E-15	0.782585	0.000472	0.212152	0.000288	0.002562	0.000061	0.002437	0.000091	0.000084	0.000006	96.85	3.572583	0.00967	97.96	± 0.52	37.4	xenocryst
6	5.126E-15	0.868443	0.000661	0.241747	0.000271	0.002907	0.000068	0.001856	0.000067	0.000070	0.000005	97.64	3.507456	0.00809	96.22	± 0.43	56.0	xenocryst
7	4.144E-15	0.702153	0.000606	0.198267	0.000228	0.002390	0.000042	0.001283	0.000065	0.000055	0.000005	97.72	3.460709	0.00943	94.97	± 0.50	66.4	
8	5.745E-15	0.973411	0.000506	0.276142	0.000362	0.003401	0.000049	0.002232	0.000065	0.000043	0.000006	98.71	3.479759	0.00829	95.48	± 0.44	53.2	
9	2.338E-15	0.396142	0.000515	0.108011	0.000164	0.001323	0.000045	0.000792	0.000050	0.000069	0.000006	94.90	3.480665	0.01686	95.51	± 0.90	58.7	< 95%*40Ar
10	3.261E-15	0.552588	0.000462	0.155062	0.000195	0.001876	0.000055	0.001222	0.000074	0.000040	0.000005	97.88	3.487987	0.01119	95.70	± 0.60	54.5	
11	9.995E-16	0.169353	0.000184	0.046022	0.000109	0.000596	0.000029	0.000517	0.000141	0.000005	0.000006	99.23	3.651335	0.04125	100.07	± 2.20	38.3	xenocryst
12	1.263E-15	0.213998	0.000284	0.060697	0.000098	0.000707	0.000037	0.000809	0.000122	0.000012	0.000006	98.36	3.467831	0.03023	95.16	± 1.62	32.3	
13	5.841E-16	0.098965	0.000144	0.027963	0.000085	0.000351	0.000031	0.000256	0.000131	0.000009	0.000006	97.46	3.449200	0.06199	94.67	± 3.32	47.0	
14	6.021E-16	0.102023	0.000144	0.029188	0.000079	0.000351	0.000032	0.000310	0.000137	0.000005	0.000006	98.57	3.445468	0.06020	94.57	± 3.22	40.4	
15	9.542E-16	0.161678	0.000215	0.046125	0.000097	0.000548	0.000026	0.000199	0.000150	0.000007	0.000007	98.66	3.458240	0.04285	94.91	± 2.29	99.8	
16	2.298E-15	0.389338	0.000336	0.111399	0.000159	0.001334	0.000047	0.000846	0.000160	0.000001	0.000006	99.94	3.492830	0.01722	95.83	± 0.92	56.6	
17	1.458E-15	0.247044	0.000297	0.070100	0.000103	0.000844	0.000027	0.000699	0.000129	0.000006	0.000006	99.25	3.497903	0.02481	95.97	± 1.33	43.1	
18	7.433E-16	0.125944	0.000160	0.035729	0.000084	0.000427	0.000026	0.000161	0.000132	0.000017	0.000006	96.06	3.386311	0.04919	92.98	± 2.63	95.5	
19	3.097E-15	0.524800	0.000410	0.082133	0.000127	0.001178	0.000032	0.000906	0.000147	0.000823	0.000009	53.70	3.430954	0.03407	94.18	± 1.82	39.0	< 95%*40Ar
20	1.806E-15	0.306002	0.000270	0.087089	0.000124	0.001085	0.000030	0.000527	0.000147	0.000006	0.000006	99.44	3.494119	0.02125	95.87	± 1.14	71.0	
21	1.213E-15	0.205480	0.000207	0.059073	0.000098	0.000660	0.000045	0.002098	0.000159	0.000006	0.000006	99.24	3.452244	0.03067	94.75	± 1.64	12.1	
22	1.214E-15	0.205704	0.000243	0.058522	0.000111	0.000753	0.000022	0.000807	0.000142	0.000010	0.000006	98.61	3.466081	0.02950	95.12	± 1.58	31.2	
23	8.809E-16	0.149251	0.000221	0.042557	0.000094	0.000534	0.000030	0.000286	0.000162	0.000002	0.000006	99.65	3.494958	0.04159	95.89	± 2.22	64.0	
24	1.816E-15	0.307701	0.000285	0.088126	0.000175	0.001002	0.000053	0.000671	0.000143	0.000010	0.000006	99.06	3.458638	0.02183	94.92	± 1.17	56.5	
25	9.000E-16	0.152484	0.000191	0.043313	0.000098	0.000523	0.000045	0.000289	0.000147	0.000003	0.000006	99.36	3.498187	0.04306	95.98	± 2.30	64.5	
26	1.809E-15	0.306501	0.000291	0.088112	0.000152	0.001078	0.000037	0.000748	0.000136	0.000001	0.000006	99.92	3.475934	0.02273	95.38	± 1.22	50.7	
27	2.067E-15	0.350183	0.000257	0.099209	0.000164	0.001232	0.000042	0.000677	0.000161	0.000019	0.000006	98.42	3.474025	0.01795	95.33	± 0.96	63.0	
28	2.369E-15	0.401463	0.000348	0.114714	0.000180	0.001358	0.000046	0.000875	0.000141	0.000001	0.000007	99.92	3.496999	0.01788	95.94	± 0.96	56.4	
29	7.905E-16	0.133942	0.000152	0.035896	0.000089	0.000437	0.000034	0.000485	0.000138	0.000035	0.000006	92.36	3.446373	0.04794	94.59	± 2.56	31.8	< 95%*40Ar
30	1.896E-15	0.321286	0.000252	0.091224	0.000159	0.001085	0.000028	0.000940	0.000138	0.000015	0.000006	98.62	3.473243	0.02136	95.31	± 1.14	41.7	
31	2.271E-15	0.384812	0.000280	0.110047	0.000149	0.001225	0.000042	0.001002	0.000160	0.000001	0.000006	99.97	3.495711	0.01692	95.91	± 0.90	47.2	
32	1.747E-15	0.295985	0.000279	0.084498	0.000156	0.000984	0.000049	0.000494	0.000143	0.000001	0.000006	99.95	3.501162	0.02317	96.06	± 1.24	73.6	
33	2.383E-15	0.403723	0.000274	0.115874	0.000156	0.001457	0.000056	0.000714	0.000143	0.000005	0.000006	99.62	3.471019	0.01621	95.25	± 0.87	69.8	
													weighted mean age (25 of 33):		95.39	± 0.18		

The values in this table represent blank, discrimination, and decay (^{37}Ar and ^{39}Ar) corrected values.

Atmospheric argon ratios

$^{40}Ar/^{36}Ar$	295.5 ± 0.5	Steiger & Jäger (1977)
$^{38}Ar/^{36}Ar$	0.1880 ± 0.0003	Nier (1950)

Interfering isotope production ratios

$(^{40}Ar/^{39}Ar)_K$	$(5.4 \pm 1.4) \times 10^{-4}$	Jicha and Brown (2013)
$(^{38}Ar/^{39}Ar)_K$	$(1.210 \pm 0.002) \times 10^{-2}$	Jicha and Brown (2013)
$(^{39}Ar/^{37}Ar)_{Ca}$	$(6.95 \pm 0.09) \times 10^{-4}$	Renne et al. (2013)
$(^{38}Ar/^{37}Ar)_{Ca}$	$(1.96 \pm 0.08) \times 10^{-5}$	Renne et al. (2013)
$(^{36}Ar/^{37}Ar)_{Ca}$	$(2.65 \pm 0.022) \times 10^{-4}$	Renne et al. (2013)

Decay constants

λ_{40Ar}	$(0.580 \pm 0.014) \times 10^{-10}\ a^{-1}$	Min et al. (2000)
λ_{B-}	$(4.884 \pm 0.099) \times 10^{-10}\ a^{-1}$	Min et al. (2000)
^{39}Ar	$(2.58 \pm 0.03) \times 10^{-3}\ a^{-1}$	Stoenner et al. (1965)
^{37}Ar	$(5.4300 \pm 0.0063) \times 10^{-2}\ a^{-1}$	Renne & Norman (2001)
$^{36}Cl\ \lambda_B$	$(2.35 \pm 0.02) \times 10^{-6}\ a^{-1}$	Endt (1998)

REFERENCES

Endt, P.M., 1998, Supplement to energy levels of A= 21-44 nuclei (VII): Nuclear Physics A, v. 633, no. 1, p. 1-220.

Jicha, B.R., and Brown, F.H., 2013, An age for the Korath Range, Ethiopia and the viability of $^{40}Ar/^{39}Ar$ dating of kaersutite in Late Pleistocene volcanics, Quaternary Geochronology, v.21, p. 53-57.

Joo, Y.J., Sageman, B.B. and Hurtgen, M.T., 2014, in press, Cenomanian to Campanian Carbon Isotope Record from the Western Interior Basin, Journal of Sedimentary Research.

Laskar, J., Robutel, P., Joutel, F., Gastineau, M., Correia, A.C.M., Levrard, B., 2004, A long-term numerical solution for the insolation quantities of the Earth, Astronomy & Astrophysics, v. 428, p. 261-285.

Laskar, J., Fienga, A., Gastineau, M., Manche, H., 2011. La2010: A new orbital solution for the long-term motion of the Earth. Astron. Astrophys., v. 532, p. A89.

Meyers, S.R., Sageman, B.B., Arthur, M.A., 2012b. Obliquity forcing of organic matter accumulation during Oceanic Anoxic Event 2. Paleoceanography, v. 27, PA3212, doi:10.1029/2012PA002286.

Min, K., Mundil, R., Renne, P.R., Ludwig, K.R., 2000. A test for systematic errors in $^{40}Ar/^{39}Ar$ geochronology through comparison with U/Pb analysis of a 1.1-Ga rhyolite. Geochimica et Cosmochimica Acta, v. 64, p. 73-98.

Nier A.O., 1950. A redetermination of the relative abundances of the isotopes of carbon, nitrogen, oxygen, argon, and potassium. Phys. Rev. v. 77, p. 789–793.

Potts, P. J., Tindle A. G., Webb P. C., 1992. Geochemical Reference Material Compositions: Rocks, Minerals, Sediments, Soils, Carbonates, Refractories & Ores Used in Research & Industry. Whittles Pub, Latheronwheel, Caithness, U.K., Whittles Publishing, 313 p.

Renne P.R. and Norman E.B., 2001, Determination of the half-life of ^{37}Ar by mass spectrometry: Physical Review C, v. 63, p. 047302-1– 047302-3.

Renne, P.R., Deino, A.L., Hilgen, F.J., Kuiper, K.F., Mark, D.F., Mitchell, W.S. III, Morgan, L.E., Mundil, R., Smit, J., 2013, Time Scales of Critical Events Around the Cretaceous-Paleogene Boundary, Science, v. 339, p. 684-687.

Steiger, R.H., and Jäger, E., 1977, Subcommission on Geochronology: Convention on the use of decay constants in geo- and cosmochronology: Earth and Planetary Science Letter, v. 36, p. 359-362.

Stoenner, R.W., Schaeffer, O.A., and Katcoff, S., 1965, Half-lives of argon-37, argon-39 and argon-42: Science, v. 148, p. 1325-1328.